Chinese Chemical Letters 35 (2024) 108656

Contents lists available at ScienceDirect

Chinese Chemical Letters

journal homepage: www.elsevier.com/locate/cclet

Glutathione-depleted cyclodextrin *pseudo*-polyrotaxane nanoparticles for anti-inflammatory oxaliplatin (IV) prodrug delivery and enhanced colorectal cancer therapy

Wenjia Wang[a,1], Xingyue He[a,1], Xiaojie Wang[a,1], Tiantian Zhao[a], Osamu Muraoka[b], Genzoh Tanabe[b], Weijia Xie[c], Tianjiao Zhou[a], Lei Xing[a,*], Qingri Jin[d,*], Hulin Jiang[a,e,*]

[a] State Key Laboratory of Natural Medicines, China Pharmaceutical University, Nanjing 210009, China
[b] Faculty of Pharmacy Kinki University, Higashiosaka, Osaka 577-8502, Japan
[c] State Key Laboratory of Natural Medicines (SKLNM) and Department of Medicinal Chemistry, School of Pharmacy, China Pharmaceutical University, Nanjing 210009, China
[d] School of Pharmacy, Hangzhou Medical College, Hangzhou 311399, China
[e] College of Pharmacy, Yanbian University, Yanji 133002, China

ARTICLE INFO

Article history:
Received 5 May 2023
Revised 1 June 2023
Accepted 4 June 2023
Available online 7 June 2023

Keywords:
Oxaliplatin
Glutathione depletion
Tetravalent platinum prodrug
Synergistic therapy
Colorectal cancer

ABSTRACT

Oxaliplatin (Oxa) is the first-line chemotherapeutic drug for the treatment of colorectal cancer (CRC). However, long-term Oxa chemotherapy can induce inflammation and increase the levels of cyclooxygenase-2 (COX-2) and prostaglandin E2 (PGE2), which can promote tumor metastasis. Moreover, high glutathione (GSH) levels in CRC cells significantly reduce Oxa sensitivity and seriously restrict the clinical application of Oxa. Herein, an Oxa(IV) prodrug with anti-inflammatory properties (desmethyl naproxe, DN) and GSH-depleting cyclodextrin *pseudo*-polyrotaxane carriers were prepared and further self-assembled into micellar nanoparticles (designated DNPt@PPRI). The relesae of DN from DNPt@PPRI can reduce the level of PGE2 to inhibit inflammation and tumor metastasis by decreasing COX-2 protein, and also synergize with Oxa to inhibit tumor. More importantly, GSH depletion can reduce the detoxification of Oxa and further enhance chemotherapy-induced apoptosis. DNPt@PPRI have a good GSH depletion ability to enhance the sensitivity of Oxa, indicating a potential in the synergistic chemotherapy and chemo-sensitization of colorectal cancer.

Colorectal cancer (CRC) is the third most common malignancy and the third most common cause of cancer-related death worldwide [1,2]. There is an overall shift towards advanced disease, with more people being diagnosed at advanced stages, according to the most recent CRC data in 2023 [3]. Chemotherapy is one of the most effective methods for the treatment of CRC besides surgery. However, due to the high metastasis of CRC, the overall survival rate of metastatic CRC treated with chemotherapy is only 10.8% [4,5]. Therefore, more effective treatments for CRC must be developed.

Oxaliplatin (Oxa), the third generation of platinum-based antitumor agents, is widely used in the treatment of advanced CRC [6]. Oxa can cause functional damage of DNA by interfering with DNA replication and transcription through nuclear DNA adduct formation [7]. However, studies have shown that Oxa can increase the level of inflammatory cytokines, such as interleukin 6 (IL-6) and cyclooxygenase-2 (COX-2), which are highly expressed in colorectal cancer [8–10]. And the presence of inflammatory response is also associated with poor response to chemotherapeutic drugs [11]. Prostaglandin E2 (PGE2), a downstream factor of COX-2, has been found to promote tumor cell growth and enhance tumor immune evasion, leading to tumor more aggressive [12,13]. PGE2 can interact with tumor microenvironment related cells, such as tumor-associated macrophages, fibroblasts, and neutrophils, and promote the high expression of tumor metastasis signaling pathways such as vascular endothelial growth factor (VEGF) and extracellular regulated protein kinase (ERK) pathways. Non-steroidal anti-inflammatory drugs (NSAIDs) have been proved to inhibit the production of COX-2, which can reduce the risk and recurrence of CRC [14–16].

On the other hand, one of the most important reasons for the unsatisfactory antitumor effect of chemotherapy is the cy-

* Corresponding authors.
E-mail addresses: xinglei6xl@163.com (L. Xing), jinqr@hmc.edu.cn (Q. Jin), jianghulin3@163.com (H. Jiang).
[1] These authors contributed equally to this work.

https://doi.org/10.1016/j.cclet.2023.108656
1001-8417/

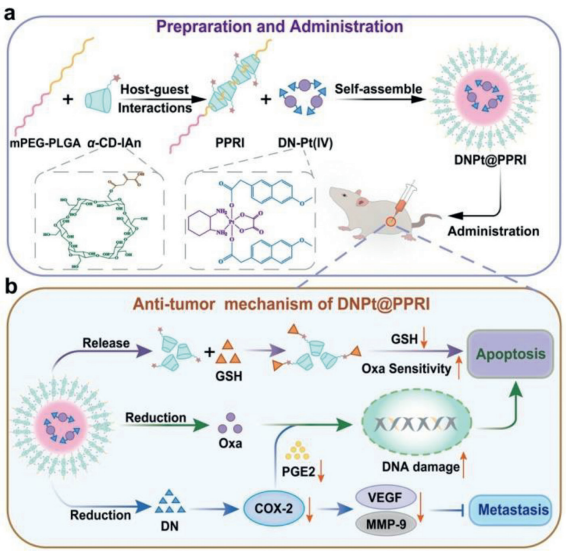

Scheme 1. (a) The fabrication of DNPt@PPRI and (b) the anti-tumor mechanism of DNPt@PPRI in CRC.

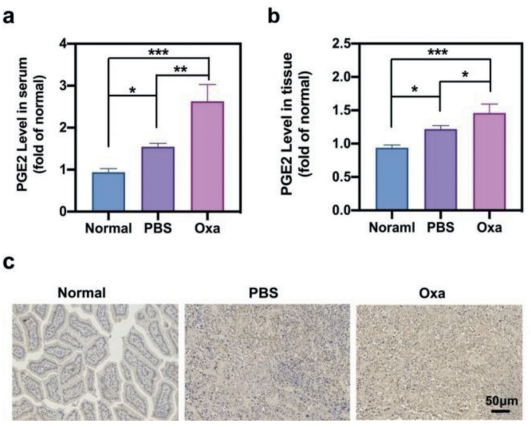

Fig. 1. PGE2 levels in serum (a) and colon tissues (normal) or tumors (PBS, Oxa) (b). (c) Immunohistochemistry of COX-2 in colon tissues (normal) or tumors (PBS, Oxa). Mean ± standard deviation (SD) ($n = 3$. $^{*}P < 0.05$, $^{**}P < 0.01$, $^{***}P < 0.001$).

tosolic detoxification of Oxa. Glutathione (GSH) is the most abundant sulfhydryl-containing molecule in tumor cells and can bind tightly to Pt to form Pt-GSH conjugates, which are rapidly exported from tumor cells by ATP-dependent glutathione *S*-conjugate export pumps [17,18]. A large number of studies have proved that the chemotherapy sensitivity of Oxa could be restored and the active amount of Oxa in cancer cells can be enhanced by downregulating the intracellular GSH concentration [19–22]. In addition, itaconic anhydride (IAn) has been shown to reduce intracellular GSH levels through double bond and sulfhydryl group reaction, therefore it can be used as a GSH inhibitor [23]. In addition, the strategy of delivering platinum prodrugs through nano-systems has been widely studied. Nano-systems can assemble drugs and functional carriers into delivery systems to work together to enhance the efficacy of drugs [24–26]. Therefore, we used nano-systems to enhance the anti-tumor efficacy of Oxa, this strategy might greatly enhance the treatment of colorectal cancer.

In this study, we constructed a GSH-depleted cyclodextrin *pseudo*-polyrotaxane nano-system to deliver anti-inflammatory Oxa(IV) prodrug for CRC treatment (Scheme 1a). First, we assembled α-cyclodextrin-itaconic anhydride (α-CD-IAn) and methoxy poly(ethylene glycol)-poly(L-lactide-*co*-glycolide) (mPEG-PLGA) into *pseudo*-polyrotaxane (PPRI) by host–guest interaction [27,28]. After that, anti-inflammatory Oxa(IV) prodrug (DN-Pt(IV)) was loaded into the PPRI nano-system by nanoprecipitation to form the final preparation DNPt@PPRI. As shown in Scheme 1b, upon uptake of DNPt@PPRI by tumor cells, the DN-Pt(IV) prodrug could be responsively reduced and released free Oxa and desmethyl naproxe (DN) under the high GSH environment of the tumor. Subsequently, Oxa could cause DNA damage, leading to apoptosis. The release of DN inhibited the expression of COX-2, then down-regulated the level of PGE2 and metastasis-related proteins VEGF, matrix metallopeptidase 9 (MMP-9) to enhance Oxa-induced apoptosis and inhibit tumor metastasis. IAn in the vector further consumed intracellular GSH and inhibited the detoxification of the tumor to Oxa, enhancing chemotherapy sensitivity. Therefore, DNPt@PPRI could effectively ameliorate the inactivation of Oxa, and possess potent dual anti-tumor effects when combined with COX-2 inhibitors.

Firstly, to demonstrate the necessity of Oxa combined with COX-2 inhibitors, we first investigated the expression of PGE2 of tumor tissues in BALB/c mice after Oxa treatment, and compared it with healthy mice and phosphate buffered saline (PBS) treated tumor-bearing mice. The animal experiments were approved by the Ethics Committee of China Pharmaceutical University. The results showed that PGE2 level of PBS group was higher than that of normal group in tumor tissue and serum, while that of Oxa group was significantly higher than that in PBS and normal group (Figs. 1a and b). As shown in Fig. 1c, after Oxa treatment, COX-2 content in tumor tissues was significantly upregulated, this also further confirmed that long-term chemotherapy could aggravate the inflammatory microenvironment of colon cancer, and promote the generation of downstream factor PGE2, which may promote tumor proliferation and metastasis. These results are consistent with literature reports [29]. Therefore, Oxa combined with COX-2 inhibitors is a viable treatment strategy for colorectal cancer.

Before drug synthesis, we investigated the synergistic effect of Oxa and DN (Fig. 2a), the results showed that the synergistic effect was the strongest when the ratio was 1:2 [30]. The specific synthesis method of DN-Pt(IV) prodrug was shown in Fig. S1 (Supporting information) [31–33]. The successful synthesis of DN-Pt(IV) was confirmed by electro spray ionization-mass spectroscopy (ESI-MS) (Fig. S2 in Supporting information), ^{1}H and ^{13}C nuclear magnetic resonance spectroscopy (^{1}H NMR and ^{13}C NMR) (Fig. S3 in Supporting information), and ultraviolet–visible spectrophotometry (UV–vis) (Fig. S4 in Supporting information) [34–36]. High GSH can induce activation of Pt(IV) into active Pt(II) from DN-Pt(IV). Therefore, PBS (pH 7.4) + 10 mmol/L GSH was used as simulated medium to evaluate the reactivity of DN-Pt(IV) in the reduced intracellular environment [37]. As shown in Fig. S5 (Supporting information), the ESI-MS analysis confirmed the existence of typical peaks of $[Oxa(II)+H]^{+}$ (*m/z*, 396.01) and $[Oxa(II)+Na]^{+}$ (*m/z*, 411.98) under reduction condition. It indicated that Pt-O bond was broken and Oxa was released in DN-Pt(IV).

To further improve the properties of DN-Pt(IV) prodrug, we constructed cyclodextrin *pseudo*-polyrotaxanes for delivery of prodrug. Before that, IAn was modified on α-CD to deplete GSH. The synthesis route of α-CD-IAn was shown in Fig. S6 (Supporting information). The successful synthesis of α-CD-IAn was identified by matrix-assisted laser desorption/ionization time-of-flight mass spectrometry (MALDI-TOF MS) (Fig. S7 in Supporting information), ^{1}H NMR (Fig. S8 in Supporting information), and Fourier transform infrared spectroscopy (FT-IR) (Fig. S9 in Supporting information) [38]. As shown in Fig S10 (Supporting information), after 12 h of treatment with IAn or α-CD-IAn, the intracellular GSH level was reduced by 40% compared to the control group, while there was little change in the α-CD group. Finally, α-CD-IAn was inserted into the PEG chain of mPEG-PLGA to form *pseudo*-polyrotaxanes

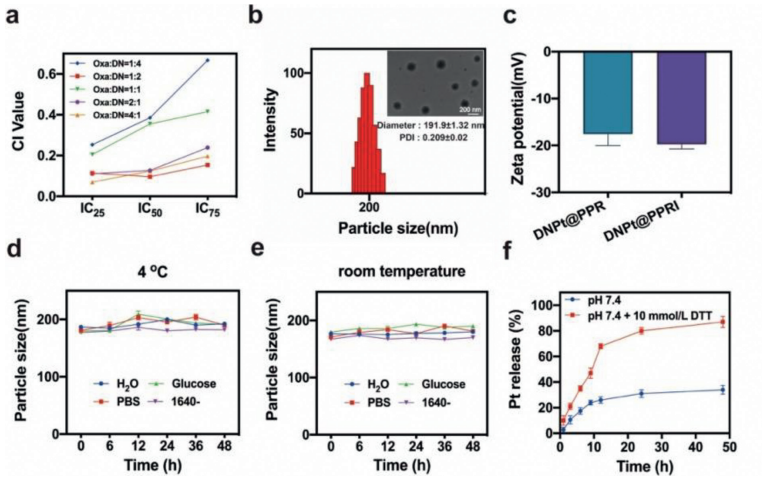

Fig. 2. (a) CI value in different ratios of physical mixture between Oxa and DN. (b) Size distribution and TEM image (inserted) of DNPt@PPRI. Scale bar: 200 nm. (c) Zeta potentials of DNPt@PPR and DNPt@PPRI. (d) The stability of DNPt@PPRI at 4 °C and (e) room temperature. (f) Release profile of DNPt@PPRI in phosphate buffer at pH 7.4 and pH 7.4 + 10 mmol/L DTT. Mean ± SD ($n = 3$).

[39]. The IAn modified *pseudo*-polyrotaxane was named PPRI, and the unmodified *pseudo*-polyrotaxane was named PPR. As shown in Fig. S11 (Supporting information), PPRI and PPR have multiple characteristic peaks of the repeating unit PEG and α-CD, which showed that *pseudo*-polyrotaxane was successfully self-assembled [40]. According to the X-ray diffraction (XRD) results (Fig. S12 in Supporting information), PPR and PPRI have a clear crystal peak at $2\theta = 19.7°$, which is the characteristic crystal peak of α-CD self-assembly with polymer chain to form inclusion complex, which also confirmed the successful preparation of *pseudo*-polyrotaxane. As shown in Fig. S13 (Supporting information), the cell survival rates with different functions were above 80%, indicating that the *pseudo*-polyrotaxane has good safety and is conducive to the delivery of DN-Pt (IV) prodrug.

Based on the above, DNPt@PPRI were prepared by nano precipitation method [41]. The results of the prescription screening were shown in Figs. 2b and c and Table S1 (Supporting information), the particle size of DNPt@PPRI is 191.9 ± 1.32 nm, the polymer dispersity index (PDI) is 0.209 ± 0.02, and the zeta potential is −19.74 ± 1.01 mV. DNPt@PPR had a particle size of 176.1 ± 3.71 nm, PDI value of 0.246 ± 0.01, and zeta potential of −17.53 ± 2.48 mV. DNPt@PPRI images taken by transmission electron microscope (TEM) show that the appearance of the nanoparticles was basically spherical and consistent with previous measurements [42]. In addition, we also investigate the stability of DNPt@PPRI with time in different media and at different temperatures. The results were shown in Figs. 2d and e. DNPt@PPRI were dispersed in 5% glucose, PBS, distilled water and 1640 medium, and showed good stability at room temperature or 4 °C. Inductively coupled plasma-mass spectrometry (ICP-MS) analysis showed that the amount of Pt released by DNPt@PPRI increased after 48 h incubation in PBS (pH 7.4) +10 mmol/L DTT, reaching 80%, much higher than PBS alone (pH 7.4) (Fig. 2f). This indicated that the DN-Pt(IV) prodrug released free Oxa under reductive condition, which was conducive to the accumulation of the drug at the tumor site. Then, we studied the process of DNPt@PPRI escaping from lysosomes [43]. As shown in Fig. S14 (Supporting information), green and red fluorescence overlapped at 4 h, and they were at different positions at 8 h, indicating the escape of nanoparticles from lysosomes. This result indicated that the nanoparticles could escape from lysosomes and avoid being degraded.

Afterwards, we evaluated the anti-tumor activity of DNPt@PPRI *in vitro*. The toxicity of DNPt@PPRI in three CRC cell lines was detected by MTT assay (Fig. 3a) [44], and half maximal inhibitory concentration (IC_{50}) values of cells treated with different drugs were calculated (Table S2 in Supporting information). The IC_{50} of DNPt@PPRI for CT-26 and HCT-116 cells were 22.34 and 12.11 times that of Oxa, and 47.73 times that of HT-29 cells. DNPt@PPRI is far more effective than Oxa in tumor killing, and it can achieve the same therapeutic effect as Oxa at lower dose [45]. Meanwhile, the therapeutic effect of DNPt@PPRI was better than that of DNPt@PPR group, meaning that GSH depletion could promote anti-tumor efficacy. In addition, the results of live/dead cell staining in Fig. 3b showed that the free Oxa, DN and mixed groups showed weak red fluorescence after treatments, while the DNPt@PPRI group showed a large amount of red fluorescence, which was stronger than that of DNPt@PPR group, indicating that DNPt@PPRI had significant cell killing effect. The results of trypan blue staining were consistent with the live/dead cell staining, DNPt@PPRI group showed more purple color, indicating that the integrity and permeability of the cell membrane were disrupted, resulting in massive cell death. Nuclear contraction and DNA fragmentation were observed by Hoechst 33342 staining in Fig. S15 (Supporting information), further illustrating that DNPt@PPRI had high cytotoxic effect. After that, we examined the anti-metastasis ability of DNPt@PPRI by cell scratch and migration assays [46]. As shown in Fig. 3c (i and ii), cells treated without drugs had strong scratch healing ability and migration ability. Oxa group was similar to control group, indicating that Oxa had no effect on tumor metastasis. The abilities to inhibit metastasis were weak in DN and mixture groups, while DNPt@PPRI group was significantly greater than that in DNPt@PPR and mixture groups. These results indicated that DNPt@PPRI had good anti-tumor activity *in vitro* and positive implications for colorectal cancer therapy.

Furthermore, we elucidated the anti-tumor mechanism of DNPt@PPRI. First, we studied reactive oxygen species (ROS) production in cells by using 2′,7′-dichlorodihydrofluorescein diacetate (DCFH-DA) probe [47,48]. High ROS levels lead to a cascade of reactions, including lipid peroxidation, protein destruction, and DNA destruction, leading to cell death [49,50]. As shown in Fig. 4a and corresponding quantitative results in Fig. 4b, green fluorescence intensity was significantly enhanced after treatment with DNPt@PPRI, which was higher than that in DNPt@PPR groups, showing a significant difference compared with other groups. Then, the results of JC-1 staining and quantitative results (Figs. 4a and c) showed that the green fluorescence intensity of DNPt@PPRI group was the strongest, indicating that DNPt@PPRI could induce a sharp decrease in mitochondrial membrane potential [51]. When the

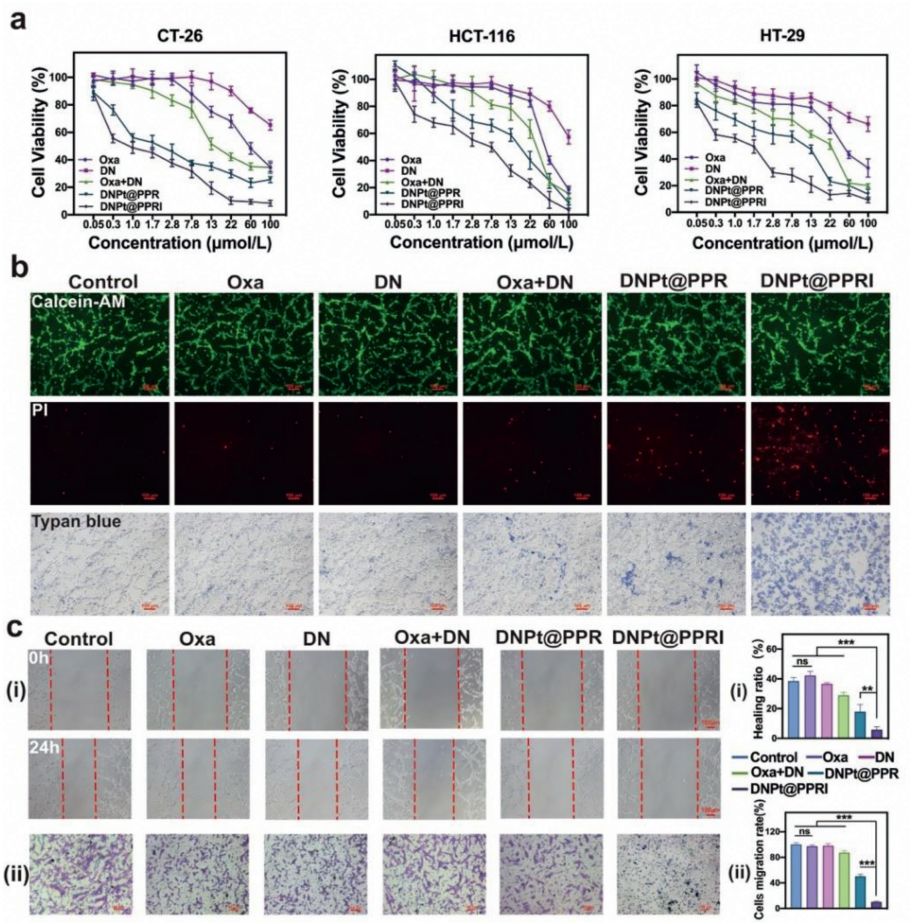

Fig. 3. Anti-tumor activity of DNPt@PPRI *in vitro*. (a) Cytotoxicity of various formulations as determined by the MTT assay in CT-26 cells. (b) Calcein-AM/propidium iodide (PI) double staining and Trypan blue staining of CT-26 cells after different treatments. Scale bar: 100 μm. (c) Wound healing (i) and migration assays (ii) in CT-26 cells after different treatments. Scale bar: 100 μm. Mean ± SD ($n = 3$. $^{**}P < 0.01$, $^{***}P < 0.001$. ns, no significance).

mitochondrial membrane potential decreases, the release of pro-apoptotic factors in the mitochondria will further activate caspase-3, start the caspase cascade, and eventually lead to cell apoptosis. As shown in Fig. S16 (Supporting information), the highest caspase-3 enzyme activity was observed in the DNPt@PPRI showed a significant ability to induce apoptosis [52–54]. In addition, Oxa can exert cytotoxicity through forming Pt-DNA adducts, leading to DNA damage [55]. The expression of phosphorylated histone H2AX (γ-H2AX) reflects the degree of DNA damage. As shown in Fig. 4a, the red fluorescence of CT-26 cells in DNPt@PPRI group was most obvious, indicating that DNPt@PPRI could induce a large amount of DNA damage. As shown in Fig. 4d, the content of GSH in tumor cells was determined, it was found that DNPt@PPRI could effectively consume intracellular GSH due to the presence of IAn. Then, intracellular platinum content was determined by ICP-MS (Fig. 4e) [56,57]. The results showed that the intracellular inactivation of Oxa was effectively reduced by depletion of GSH, resulting in a higher intracellular Pt accumulation in DNPt@PPRI than in DNPt@PPR, free Oxa, and mixed groups, supporting the importance of GSH depletion in enhancing Oxa sensitization to tumors.

Next, we observed an increase of intracellular COX-2 expression in Oxa group compared with the control after TNF-α pretreatment (Fig. 4f). The COX-2 content was down-regulated to varying degrees in other groups, and the effect of the DNPt@PPRI group was the most obvious. The expression of metastasis-related proteins was then examined by Western blot. As shown in Figs. 4g and h, the expression of VEGF and MMP-9 was significantly down-regulated in cells treated with DNPt@PPRI, which was consistent with the decreasing trend of COX-2 expression. This result suggests that COX-2 inhibition could enhance VEGF pathway blockade to inhibit angiogenesis, and down-regulate MMP-9 expression, thereby inhibiting cell invasion and metastasis [58,59]. In summary, DNPt@PPRI exhibited superior anti-tumor effects over Oxa, mainly due to the synergistic effect of Oxa with DN in DNPt@PPRI nano-delivery system and the ability to deplete GSH. These effects of DNPt@PPRI could increase the level of intracellular ROS and induce the mitochondrial apoptotic pathway, then lead to tumor cell apoptosis. It is suggested that GSH depletion and synergistic treatment are necessary for enhanced anti-tumor effects.

Based on the studies that DNPt@PPRI had a good anti-tumor effect *in vitro*, we constructed tumor-bearing mice for anti-tumor experiments *in vivo*. Mouse colorectal cancer cell line CT-26 was used to construct a tumor-bearing mouse model and different formulations were injected intratumorally every three days for five times (Fig. S17 in Supporting information) [60,61]. The survival state of the mice was observed every two days, and the weight was measured. As shown in the curve of weight change over time in Fig. 5a, the body weight of mice in Oxa and the mixture groups decreased slightly, it indicates that Oxa has some toxicity. However, in the other groups, there was no significant change in body weight during the treatment cycle, which preliminarily indicated that DNPt@PPRI had good safety *in vivo*. Tumor suppression results showed that the DNPt@PPRI group had the lowest tumor tissue weight (Fig. 5b). As shown in Fig. 5c, there was no significant difference in tumor volumes between the blank vector PPRI and PBS groups. DN group had weak anti-tumor proliferation ability.

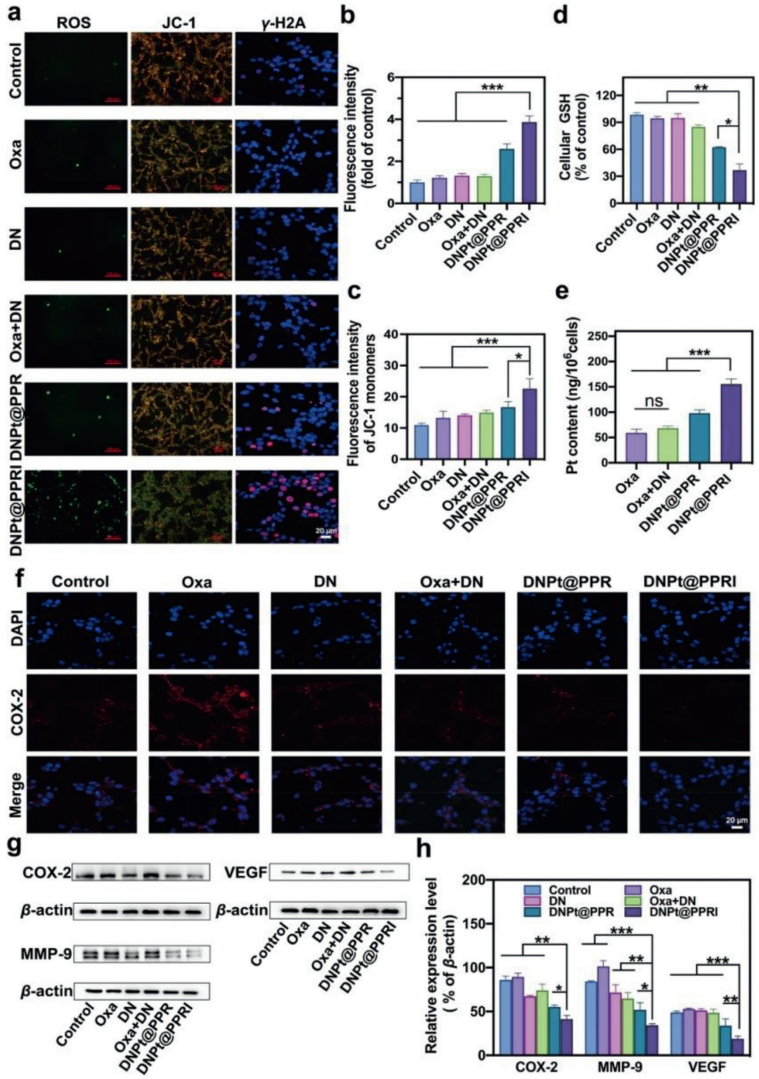

Fig. 4. The mechanism of anti-tumor effect by DNPt@PPRI. (a) Determination of intracellular ROS contents by DCFH-DA probe, JC-1 fluorescent probe staining (scale bar: 100 μm) and Immunofluorescence of γ-H2AX (scale bar: 20 μm) in CT-26 cells after treatments. (b) Fluorescence intensity of ROS ($n = 3$). (c) Fluorescence intensity of JC-1 monomers ($n = 3$). (d) Intracellular GSH level detected by GSH assay kit ($n = 3$). (e) Cellular uptake of Pt by ICP-MS ($n = 3$). (f) COX-2 expression in CT-26 cells with different formulations after TNF-α treatment. Scale bar: 20 μm. (g) Western blot analysis and quantitative analysis (h) of COX-2, MMP-9, VEGF in CT-26 cells. Mean ± SD ($n = 3$. $^{*}P < 0.05$, $^{**}P < 0.01$, $^{***}P < 0.001$). DAPI, nuclear staining with blue.

Oxa and mixture groups showed moderate anti-tumor proliferation ability. DNPt@PPR and DNPt@PPRI showed good tumor inhibition, and the tumor volume of DNPt@PPRI was the smallest. Hematoxylin and eosin (H&E) and TdT-mediated dUTP nick end labeling (TUNEL) staining results also showed that DNPt@PPRI had a good ability to induce tumor cell apoptosis and inhibit cell proliferation (Fig. 5d). As shown in Fig. S18 (Supporting information), the γ-H2AX content in the DNPt@PPRI group was significantly increased, corroborating the good anti-tumor ability of DNPt@PPRI *in vivo.*

In addition, the ability of DNPt@PPRI to inhibit lung tumor metastasis was investigated according to lung H&E staining (Fig. 5e). No obvious metastatic nodules were observed in the DNPt@PPRI treatment group compared other groups, indicating that tumor metastasis to the lung was well controlled. As shown in Fig. 5f, immunohistochemical staining of COX-2 in tumor tissues showed that COX-2 protein expression was significantly decreased after treatment with DNPt@PPRI. Next, PGE2 levels in tumor tissues and serum were detected, and the results showed that PGE2 level was up-regulated after Oxa treatment. And the level of PGE2 was significantly decreased after treatment with DNPt@PPRI, indicating that DNPt@PPRI significantly enhanced the accumulation of COX-2 inhibitors (DN) within the tumor, thereby improving the inflammatory tumor microenvironment (Figs. 5g and h). As shown in Fig. 5i, GSH content in tumor treated by DNPt@PPRI group is significantly reduced, further confirming that the strategy of GSH depletion can adequately improve the anticancer efficacy of Oxa *in vivo*. In addition, immunohistochemical staining (Fig. S19 in Supporting information) and western blot were also used to detect the expression of metastasis-related proteins (Figs. 5j and k). In the final preparation group, MMP-9 and VEGF protein expressions were significantly down-regulated compared to other groups. The above anti-tumor results *in vivo* fully demonstrated that DNPt@PPRI enhanced the anti-tumor effect of Oxa due to the GSH depletion ability, and played a strong synergistic effect with DN, thus showed the strongest anti-tumor activity *in vivo.*

H&E staining was also performed on other tissues to further investigate the biosafety of DNPt@PPRI *in vivo*. As shown in Fig. S20 (Supporting information), staining of the heart, liver, spleen and kidney in each group was normal, no pathological structural changes occurred, which showed no significant difference from

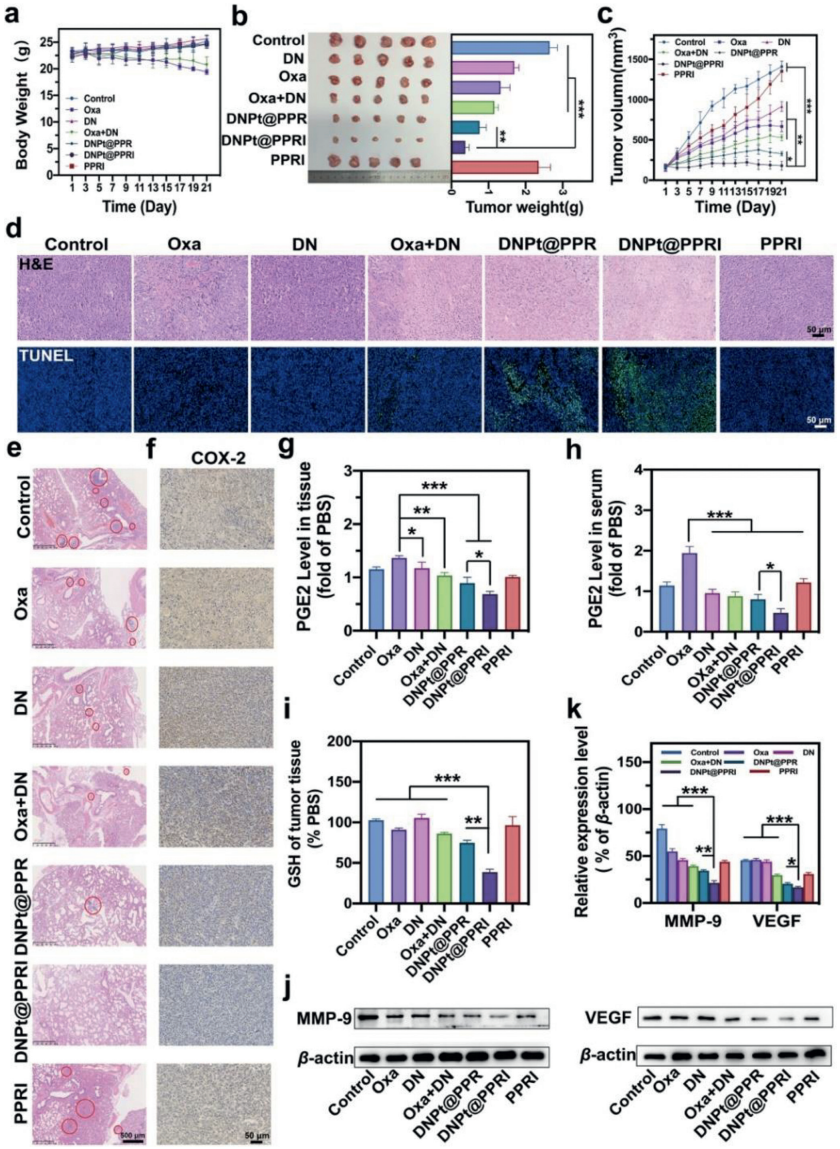

Fig. 5. Anti-tumor activity *in vivo*. (a) The body weight of mice during different treatments. (b) Images of tumor and tumor weight on day ($n = 5$). (c) The tumor volumes of mice with different treatments ($n = 5$). (d) H&E and TUNEL staining in the tumor tissues of mice after different treatments. Scale bar: 50 μm. (e) Representative images of H&E staining in lung sections. The red circles represent for the metastatic area. Scale bar: 500 μm. (f) Immunohistochemistry of COX-2 protein. Scale bar: 50 μm. (g) PGE2 levels in tumor tissues and serum (h) ($n = 3$). (i) GSH content in tumor tissues ($n = 3$). (j) Western blot analysis and quantitative analysis (k) of MMP-9, VEGF in tumor tissues. Mean ± SD ($n = 3$. $^{*}P < 0.05$, $^{**}P < 0.01$, $^{***}P < 0.001$).

the control group. This proved the safety of DNPt@PPRI. In addition, since liver and kidney are two important metabolic organs of the body, we also investigated liver hematologic indexes alanine transaminase (ALT), aspartate aminotransferase (AST), alkaline phosphatase (ALP) and kidney hematologic indexes creatinine (CRE) and blood urea nitrogen (BUN) after treatment with different drugs. As shown in Fig. S21 (Supporting information), serological indexes of all administration groups and the PBS group were at normal levels, also indicating that DNPt@PPRI did not cause damage to liver and kidney. In addition, H&E staining was normal in the blank vector group and there were no significant changes in hematological indexes, which also proved the safety of the vector.

In summary, we have rationally designed a GSH-depleting cyclodextrin *pseudo*-polyrotaxane nano-system, namely DNPt@PPRI. We synthesized GSH depletion vector loaded with anti-inflammatory Oxa(IV) prodrug for the treatment of CRC. After the nanoparticles were taken up by tumor cells, it releases Oxa and DN under the action of GSH, which induced DNA damage and down-regulation of COX-2 and PGE2 and then synergistically induced cell apoptosis and inhibited metastasis. More importantly, depletion of GSH by IAn-modified cyclodextrin *pseudo*-polyrotaxane could enhance Oxa sensitivity and improve therapeutic efficacy. Both *in vitro* and *in vivo* experiments showed that our system had strong anti-tumor ability and good biological safety. This study not only overcomes the inflammatory defect induced by Oxa chemotherapy and plays the dual anti-tumor effect of Oxa and COX-2 inhibitor, but also overcomes the limitation of easy detoxification of Oxa, which has potential application value in the clinical treatment of platinum-sensitive colorectal cancer.

Declaration of competing interest

The authors declare that they have no known competing financial interests or personal relationships that could have appeared to influence the work reported in this paper.

Acknowledgments

This work was financially supported by the National Natural Science Foundation of China (Nos. 82020108029, 82073398). This work was also supported by the Priority Academic Program Development of Jiangsu Higher Education Institutions and the Project of State Key Laboratory of Natural Medicines, China Pharmaceutical University (No. SKLNMZZ202021), the "111" Project from the Ministry of Education of China, the State Administration of Foreign Experts Affairs of China (No. B16046), and Double First-Rate construction plan of China Pharmaceutical University (Nos. CPU2018GY06, CPU2022QZ18) and China Postdoctoral Science Foundation (Nos. 2021M703598, 2022M720173), Jiangsu Funding Program for Excellent Postdoctoral Talent and International Postdoctoral Exchange Fellowship Program 2022.

Supplementary materials

Supplementary material associated with this article can be found, in the online version, at doi:10.1016/j.cclet.2023.108656.

References

[1] R.L. Siegel, K.D. Miller, N.S. Wagle, et al., CA Cancer J. Clin. 73 (2023) 17–48.
[2] N. Altoom, S.M. Ibrahim, S.I. Othman, et al., Colloids Surface A 648 (2022) 129144.
[3] R.L. Siegel, N.S. Wagle, A. Cercek, et al., CA Cancer J. Clin. 73 (2023) 233–254.
[4] L.H. Biller, D. Schrag, JAMA 325 (2021) 669–685.
[5] X.L. Chen, J. Chen, W.B. Feng, et al., Theranostics 13 (2023) 1401–1418.
[6] T. Alcindor, N. Beauger, Curr. Oncol. 18 (2011) 18–25.
[7] O.M. Alian, A.S. Azmi, R.M. Mohammad, Clin. Transl. Med. 1 (2012) 26.
[8] T. Xia, J.Z. Zhang, L.Y. Han, et al., Phytother. Res. 33 (2019) 1161–1172.
[9] Q.H. Chen, X.Y. Lu, X.Y. Zhang, J. Clin. Transl. Hepatol. 9 (2021) 81–89.
[10] A. Lasry, A. Zinger, Y. Ben-Neriah, Nat. Immunol. 17 (2016) 230–240.
[11] J.H. Park, D.C. McMillan, P.G. Horgan, et al., Cancer Treat. Rev. 40 (2014) 68–77.
[12] A.A. Bhat, S. Nisar, M. Singh, et al., Cancer Commun. 42 (2022) 689–715.
[13] C.W. Su, Y. Zhang, Y.T. Zhu, Crit. Rev. Oncol. Hematol. 107 (2016) 33–38.
[14] W.K. Chia, R. Ali, H.C. Toh, Nat. Rev. Clin. Oncol. 9 (2012) 561–570.
[15] C.R. Bell, V.S. Pelly, A. Moeini, et al., Nat. Commun. 13 (2022) 2063.
[16] L. Xing, C.X. Yang, D. Zhao, et al., J. Control. Release 331 (2021) 460–471.
[17] E. Martinez-Balibrea, A. Martinez-Cardus, A. Gines, et al., Mol. Cancer Ther. 14 (2015) 1767–1776.
[18] A. Bansal, M.C. Simon, J. Cell Biol. 217 (2018) 2291–2298.
[19] Q. Jin, S.Q. Yan, H. Hu, et al., Small Methods 5 (2021) e2101047.
[20] D.C. Qi, L. Xing, L.J. Shen, et al., Chin. Chem. Lett. 33 (2022) 4595–4599.
[21] T. Sun, G.P. Zhang, T. Ning, et al., Adv. Sci. 8 (2021) e2102256.
[22] X.D. Qian, Y.Q. Wang, H.L. Xie, et al., J. Control. Release 353 (2023) 447–461.
[23] M. Bambouskova, L. Gorvel, V. Lampropoulou, et al., Nature 556 (2018) 501–504.
[24] Y.Y. Deng, F. Jia, X.H. Chen, et al., Small 16 (2020) e2001747.
[25] R. Liu, C. Luo, Z.Q. Pang, et al., Chin. Chem. Lett. 34 (2023) 107518.
[26] F. Li, X. Zhao, H. Wang, et al., Adv. Funct. Mater. 25 (2015) 788–798.
[27] H. Huang, C.H. Dong, M.Q. Chang, et al., Exploration 1 (2021) 50–60.
[28] Y. Kang, X.M. Zhang, S. Zhang, et al., Polym. Chem. 6 (2015) 2098–2107.
[29] T. Martinez-Bernabe, J. Oliver, J. Sastre-Serra, et al., Int. J. Mol. Sci. 24 (2023) 3821.
[30] V. Banerjee, N. Sharda, J. Huse, et al., Eur. J. Pharmacol. 897 (2021) 173919.
[31] L.N. Wang, Y.J. Yu, D.S. Wei, et al., Adv. Mater. 33 (2021) e2100599.
[32] F.Y. Shen, L. Feng, Y.J. Zhu, et al., Biomaterials 255 (2020) 120190.
[33] S. Jin, N. Muhammad, Y. Sun, et al., Angew. Chem. Int. Ed. 59 (2020) 23313–23321.
[34] X.J. Gao, G.X. Lei, B. Wang, et al., Adv. Sci. 10 (2023) e2205241.
[35] D.S. Wei, Y. Huang, B. Wang, et al., Angew. Chem. Int. Ed. 61 (2022) e202201486.
[36] X. Wang, X. Wang, Z. Guo, Acc. Chem. Res. 48 (2015) 2622–2631.
[37] Y.Q. Wang, H.L. Xie, Y. Wu, et al., Adv. Mater. 34 (2022) e2110614.
[38] C. Peptu, D.A. Blaj, M. Balan-Porcarasu, et al., Polymers 14 (2022) 1436.
[39] X.H. Chen, H.Q. Gao, Y.Y. Deng, et al., ACS Nano 14 (2020) 5121–5134.
[40] J. Choi, T. Takata, H. Ajiro, Macromolecules 54 (2021) 5087–5093.
[41] C.T. Zhang, J. Li, C.X. Yang, et al., Nanomedicine 23 (2020) 102071.
[42] J. Chang, Y. Li, G. Wang, et al., Nanoscale 5 (2013) 813–820.
[43] P. Zhang, Y. Zhang, X.Y. Ding, et al., Adv. Mater. 32 (2020) e2000013.
[44] T.J. Zhou, Y. Xu, L. Xing, et al., Adv. Mater 33 (2021) e2100114.
[45] S. Goschl, E. Schreiber-Brynzak, V. Pichler, et al., Metallomics 9 (2017) 309–322.
[46] Y. Xu, L.L. Huang, Y.Y. Bi, et al., Chin. Chem. Lett. 34 (2023) 107719.
[47] Y.J. He, L. Xing, P.F. Cui, et al., Biomaterials 113 (2017) 266–278.
[48] T.J. Zhou, L. Xing, Y.T. Fan, et al., J. Control. Release 307 (2019) 44–54.
[49] T.J. Zhou, L. Xing, Y.T. Fan, et al., J. Control. Release 309 (2019) 82–93.
[50] J. Wan, X.H. Zhang, Z.H. Li, et al., Adv. Healthc. Mater. (2022) e2202710.
[51] Y. Wang, L.F. Hu, P.F. Cui, et al., Adv. Mater. 33 (2021) e2103307.
[52] D. Brenner, T.W. Mak, Curr. Opin. Cell Biol. 21 (2009) 871–877.
[53] D.F. Suen, K.L. Norris, R.J. Youle, Genes Dev. 22 (2008) 1577–1590.
[54] L.A. Pradelli, M. Beneteau, J.E. Ricci, Cell Mol. Life Sci. 67 (2010) 1589–1597.
[55] G.Y. Zhu, M. Myint, W.H. Ang, et al., Cancer Res. 72 (2012) 790–800.
[56] Y. Xu, X.X. Han, Y.Y. Li, et al., ACS Nano 13 (2019) 13445–13455.
[57] Y. Zhu, L. Xing, X. Zheng, et al., Int. J. Pharm. 573 (2020) 118736.
[58] L.H. Xu, J. Stevens, M.B. Hilton, et al., Sci. Transl. Med. 6 (2014) 242ra284.
[59] D.B. Vendramini-Costa, J.E. Carvalho, Curr. Pharm. Des. 18 (2012) 3831–3852.
[60] X.L. Fu, Y.B. Shi, H.C. Zang, et al., J. Control. Release 347 (2022) 1–13.
[61] B. Zhang, T.Q. Wang, S.M. Yang, et al., J. Control. Release 238 (2016) 10–21.